Midfield Wireless Powering of Subwavelength Autonomous Devices

Sanghoek Kim, John S. Ho, and Ada S. Y. Poon*

Department of Electrical Engineering, Stanford University, Stanford, California 94305, USA

(Received 5 December 2012; published 17 May 2013)

We obtain an analytical bound on the efficiency of wireless power transfer to a weakly coupled device. The optimal source is solved for a multilayer geometry in terms of a representation based on the field equivalence principle. The theory reveals that optimal power transfer exploits the properties of the midfield to achieve efficiencies far greater than conventional coil-based designs. As a physical realization of the source, we present a slot array structure whose performance closely approaches the theoretical bound.

DOI: 10.1103/PhysRevLett.110.203905 PACS numbers: 41.20.Jb, 88.80.ht

Efficient wireless power transfer across tissue is highly desirable for miniaturizing autonomous devices, particularly medical implants such as pacemakers, cochlear implants, and neural stimulators. Elimination of the bulky battery and its associated safety issues raises the possibility of tiny (less than 1 mm) devices that integrate sensing, stimulation, and locomotion capabilities [1]. Most existing technologies, however, are conceptually based on wireless power transfer over air [2–6]. These systems are characterized by symmetric source and receiver coils, often helically wound with highly conductive wire, coupled through a slowly changing magnetic field (typically between 100 kHz and 50 MHz) [7–11]. For tiny devices in tissue, the extreme asymmetry between source and receiver results in weak coupling, and inductive power transfer is generally very inefficient (on the order of 10^{-7}) [12].

About two orders of magnitude greater efficiency can be obtained by operating at higher frequencies. For the dielectric characteristics of most tissue types, the optimal frequency is in the low gigahertz range [13]. At several centimeters of separation, operation at such frequencies corresponds to the midfield (the region where the wavelength is comparable to separation distance). Here, the general system behavior deviates from quasistatic approximations. Both reactive and radiative modes are significant and power transfer depends on diffraction effects in tissue. Dielectric dispersion, which is negligible at lower frequencies, characterizes tissue—in most cases, relaxation losses greatly exceed both radiative and Ohmic wire losses [14,15]. Source structures that exploit the characteristics of the midfield may therefore provide significantly better performance than conventional coil-based designs.

This Letter obtains an explicit solution for the source that maximizes power transfer efficiency for the general configuration shown in Fig. 1. Building on previous work that considered infinitesimal coils (rotational current) [16], the source is represented by a general surface current density confined to an infinite plane. It can be shown from the field equivalence principle [17] that an electric current density consisting of both rotational and irrotational components is sufficient to represent an arbitrary three-dimensional source (see Supplemental Material [18]). The current density that is optimal in the resulting parameter space thus bounds the performance attainable by any physical realization of the source, including apertures enhanced with near-field plates [19] or metamaterials [10,20]. In contrast to direct optimization, a solution can be found in the equivalence form without recourse to nonanalytical techniques (e.g., evolutionary optimization) [21,22] or limitations in the investigated space. As a numerical demonstration, we solve the optimal source for parameters clinically relevant to a medical cardiac device. The theory reveals the existence of sources that outperform the best coil-based design by a factor of 4. Based on analyses of the solution, we design a slot-array source that closely approaches this optimal efficiency.

Source optimization.—The exchange of energy between the source and the receiver is described by the coupled-mode equations [23]

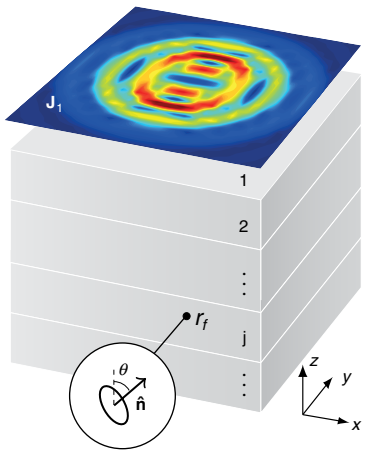

FIG. 1 (color online). The general configuration for wireless power transfer consists of a source surface current density $\mathbf{J}_1$ and a receive coil positioned in tissue with magnetic dipole moment $\hat{\mathbf{n}}$ at an angle θ. The tissue geometry is modeled by multilayers. By convention, the dipole moment aligns with the z axis when $\theta = 0°$, and the x axis when $\theta = 90°$.

$$\dot{a}_1 = (-i\omega_1 - \Gamma_1)a_1 + \kappa a_2 + F, \quad (1)$$

$$\dot{a}_2 = (-i\omega_2 - \Gamma_2 - \Gamma_L)a_2 + \kappa a_1, \quad (2)$$

where ω_n are the resonant frequencies, Γ_n the intrinsic decay rates, and a_n the amplitudes normalized such that $|a_n|^2$ correspond to the stored energy. κ is the coupling coefficient, F the driving term, and Γ_L the rate of work extraction by the load on the device. It is advantageous for the source and receiver to be in resonance $\omega := \omega_1 = \omega_2$, in which case the steady-state amplitudes have a time dependency of $\exp(-i\omega t)$ [7]. In the weakly coupled regime $|\kappa|^2 \ll \Gamma_1\Gamma_2$, the efficiency is approximately given by

$$\eta = \frac{|\kappa|^2}{\Gamma_1\Gamma_2}\frac{\Gamma_L/\Gamma_2}{(1+\Gamma_L/\Gamma_2)^2}, \quad (3)$$

which is the product of two unitless quantities: the coupling factor on the left and the matching factor on the right [12]. The matching factor is maximized when the resistance of the load and the receiver are equal $\Gamma_L = \Gamma_2$. This reproduces the impedance matching condition $R_L = R_2$, where R_L and R_2 are the real part of the load and receive coil self-impedance, from standard network theory [16]. The mismatch between R_L and R_2 can, in principle, be corrected by an impedance matching network under certain physical constraints (see Fig. S2 and related discussion in the Supplemental Material [18]).

We consider a small coil of area A_r oriented with unit normal $\hat{\mathbf{n}}$ at an angle θ with respect to the source plane. From power arguments [12], the coupling factor can be expressed as

$$\frac{|\kappa|^2}{\Gamma_1\Gamma_2} = \frac{\omega\mu_0^2 A_r^2 |\mathbf{H}_1(\mathbf{r}_f)\cdot\hat{\mathbf{n}}|^2}{R_2 \int \mathrm{Im}\epsilon(\mathbf{r})|\mathbf{E}_1(\mathbf{r})|^2 d\mathbf{r}}, \quad (4)$$

where the volume integral in the denominator extends over the entire multilayer geometry to account for all power radiated into the lower half-space. We define a parameter $\gamma/R_2 := |\kappa|^2/\Gamma_1\Gamma_2$ that characterizes the dependence on the source fields. For a fixed receiver with self-impedance R_2, optimal power transfer occurs for the particular choice of the source $\mathbf{J}_1$ that generates electromagnetic fields maximizing γ.

The multilayer tissue structure permits an analytical solution to Maxwell's equations by the angular spectrum method. Using the dyadic Green's functions, the electric and magnetic fields are given by the integral equations

$$\mathbf{E}_1(\mathbf{r}) = i\omega\mu \int \bar{\mathbf{G}}_E(\mathbf{r}-\mathbf{r}')\mathbf{J}_1(\mathbf{r}')d\mathbf{r}', \quad (5)$$

$$\mathbf{H}_1(\mathbf{r}) = \int \bar{\mathbf{G}}_H(\mathbf{r}-\mathbf{r}')\mathbf{J}_1(\mathbf{r}')d\mathbf{r}', \quad (6)$$

where $\mathbf{J}_1$ is the in-plane electric current density. The angular decompositions of $\bar{\mathbf{G}}_E$ and $\bar{\mathbf{G}}_M$ have simple forms based on the propagation of plane wave components through the multilayer geometry (see Supplemental Material [18]). Applying the Fourier transform in each of the transverse coordinates, Eqs. (5) and (6) become

$$\mathcal{E}_1(\mathbf{k}_s, z) = i\omega\mu\bar{\mathcal{G}}_E(\mathbf{k}_s, z)\mathcal{J}_1(\mathbf{k}_s), \quad (7)$$

$$\mathcal{H}_1(\mathbf{k}_s, z) = \bar{\mathcal{G}}_H(\mathbf{k}_s, z)\mathcal{J}_1(\mathbf{k}_s). \quad (8)$$

The transform variable $\mathbf{k}_s$ will be suppressed for notational simplicity. From the basic properties of the Fourier transform, the parameter γ can be rewritten as

$$\gamma = \frac{\omega\mu_0^2 A_r^2 |\int \bar{\mathcal{G}}_H(z_f)\hat{\mathbf{n}}\cdot\mathcal{J}_1 d\mathbf{k}_s|^2}{4\pi^2 \int \mathcal{J}_1^*(\int \mathrm{Im}\epsilon\bar{\mathcal{G}}_E^*(z)\bar{\mathcal{G}}_E(z)dz)\mathcal{J}_1\, d\mathbf{k}_s}. \quad (9)$$

This ratio is in the form $|\langle f, g\rangle|^2/\langle Tg, g\rangle$, where T is a bounded linear operator and $\langle f, g\rangle := \int f^* g$ for vector valued functions f and g. It is straightforward to show from the Cauchy-Schwarz inequality that if T is positive definite, then the ratio γ is maximized when $g = T^{-1}f$ (see Supplemental Material [18]) [24]. The optimum source is therefore given by

$$\mathcal{J}_{\mathrm{opt}} = \left(\int \mathrm{Im}\epsilon\bar{\mathcal{G}}_E^*(z)\bar{\mathcal{G}}_E(z)dz\right)^{-1}\bar{\mathcal{G}}_H^*(z_f)\hat{\mathbf{n}}, \quad (10)$$

corresponding to the maximum value of

$$\gamma_{\mathrm{opt}} = \frac{\omega\mu_0^2 A_r^2}{4\pi^2}\left\langle \bar{\mathcal{G}}_H^*(z_f)\hat{\mathbf{n}}, \mathcal{J}_{\mathrm{opt}}\right\rangle. \quad (11)$$

The source current density is then obtained in the spatial domain by performing an inverse Fourier transform $\mathbf{J}_{\mathrm{opt}} = \mathcal{F}^{-1}\{\mathcal{J}_{\mathrm{opt}}\}$ [25].

Numerical results.—The optimization solution does not directly yield a physical structure as a consequence of the choice of source representation. The solution, however, gives the maximum efficiency that can be obtained for a particular configuration as well as insight on how to approach this bound. We consider multilayered tissue composed of skin, fat, muscle, bone, and heart tissue (with thickness 2, 10, 8, 16 mm, and ∞, respectively). This composition approximates the typical chest wall. The receive coil has a diameter of 800 μm and the source plane is positioned 1 cm above the skin. Tissue is described by Debye relaxation $\epsilon = \epsilon_\infty + \Delta\epsilon/(1+i\omega\tau)$; the model parameters for different tissue types have been extensively tabulated [14].

To support our theoretical bound, we consider alternative source structures and verify that they result in lower efficiency. Coil sources, generated by varying the diameter of a perfectly conducting loop from 0.6 to 6 cm, serve as reference structures [26]. Other primitive structures, such as a linear dipole or uniform density result in large reactive electric fields and thus, do not yield greater efficiency. We also obtain the optimal source from Eq. (10) for frequencies ranging from 100 MHz to 4 GHz. In each case, we

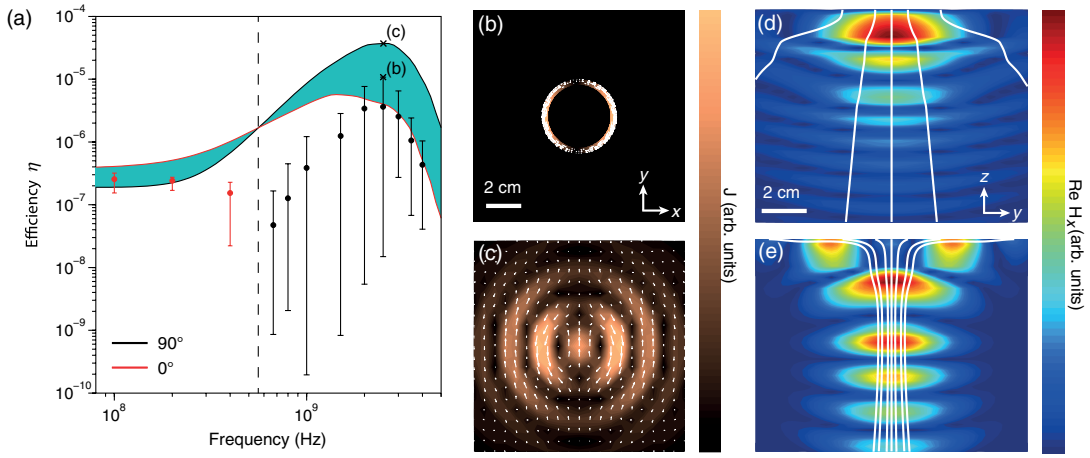

FIG. 2 (color online). (a) Theoretical bound on efficiency η for the $\theta = 90°$ (black) and the $\theta = 0°$ (red) receive coil orientations. Coil-based source structures with diameter from 0.6 to 6 cm (error bars show the max, min, and mean) achieve efficiencies well below the theoretical bound. (b)–(c) Current distribution of the coil source (top) and the optimal source (bottom) at 2.6 GHz. (d)–(e) The magnetic field component aligned with the receiver dipole moment $\hat{\mathbf{x}}$ and the Poynting vector (white) generated by the coil source (top) and the optimal source (bottom) at 2.6 GHz.

orient the receiver such that its magnetic dipole moment aligns with the dominant component of the magnetic field.

Figure 2(a) shows that the coil sources achieve efficiencies less than the bound across the entire frequency range. Frequencies less than 500 MHz correspond to the near field—the performance of the coils are within 20% of the bound in this region because the optimal source closely resembles a coil (see Fig. S3 in Supplemental Material [18]). At 2.6 GHz, where the peak efficiency occurs, the optimal source exceeds the performance of the best coil by a factor of 4, achieving an efficiency of 4×10^{-5}.

The optimal current density, shown in Fig. 2(c), does not resemble any primitive source element [27]. It exhibits the following distinctive features: (i) The current density is antisymmetric (opposing current direction) with respect to the x axis; (ii) the dominant current paths are semicircular and spaced approximately every half wavelength; (iii) the current density along each semicircular path alternates in direction and decays exponentially with radial distance. The interplay between these features results in a focusing effect, as illustrated through the component of the magnetic field responsible for power transfer in Fig. 2(e). Focusing enhances the source performance by destructively interfering with fields in directions that do not contribute to the flow of power to the receiver. In contrast, the coil source in Fig. 2(b) generates diverging power flow lines, as shown by the Poynting vector, with the maximum magnetic field occurring for the nonradiative component [Fig. 2(d)].

A reduced view of the current density is shown in Fig. 3(a). The source is composed of three primary current paths of alternating directions that evolve with time in a nonstationary manner, as shown in Fig. 3(b) over a half-period. Since the outer current paths accumulate phase linearly as they approach the center [Fig. 3(c)], the current density propagates inward. Some insight on the physical origin of the source can be obtained by considering a linear wire with a longitudinal source distribution given in Figs. 3(b) and 3(c). The beam pattern determined by the

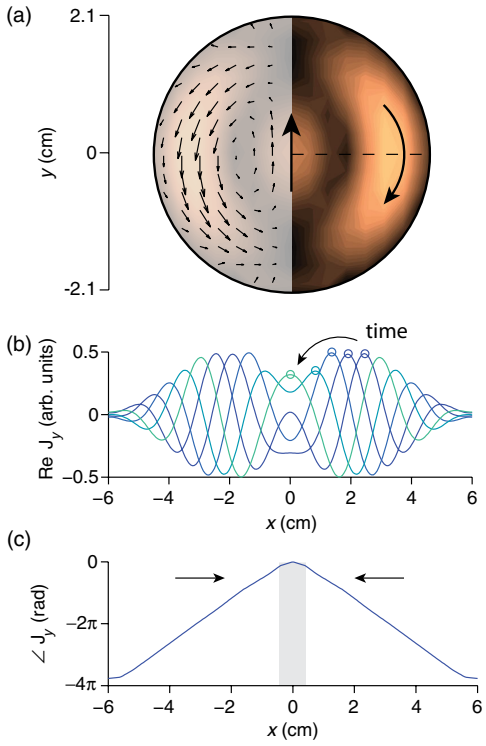

FIG. 3 (color online). (a) A reduced view of the optimal current density composed of three current paths. (b) Change in current density with time along an axial cut (dotted line) over a half-period. (c) Spatial phase variation shows that the center is stationary (constant region, shaded) while currents away from the center propagate inwards (linear region, nonshaded).

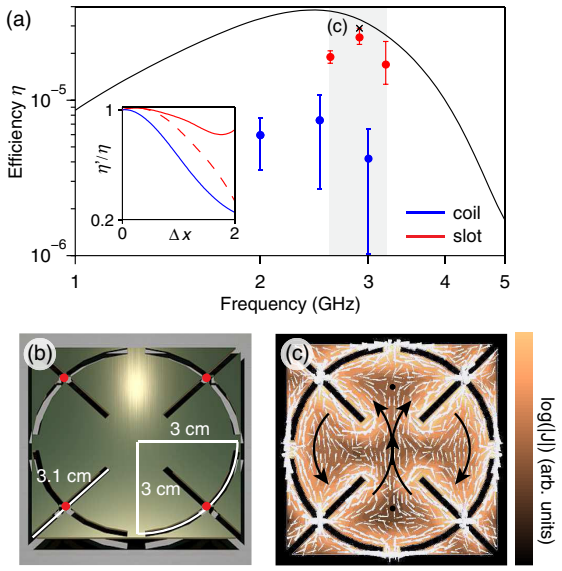

FIG. 4 (color online). (a) The slot-array efficiency (red) approaches the theoretical bound (black) and exceeds the performance of coil sources (blue). Note that the efficiency includes structural resistive losses. The slot array can be configured to be insensitive to large lateral displacements of the device (error bars show max, min, and mean from 0 to 2 cm). The inset shows the change in efficiency at 2.9 GHz for the phase-adjusted (solid red) and non-phase-adjusted (dashed red) slot array. (b) Slot array design and (c) time snapshot of the vector current density overlaying an intensity color map.

interference of radiation from each traveling wave has a conelike maximum tilted in the direction of propagation and away from the perpendicular plane [28]. Thus, the superposition of the field patterns produces crossing beams that indicate focusing in the midfield. Since sources generate identical losses in tissue regardless of distance from the receiver, the amplitude is tapered to reflect diminishing contribution to power transfer. The optimal source can be understood as a generalization of such a linear traveling wave antenna onto a surface.

Source realization.—Based on the identified features, we design a slot array structure to approximately synthesize the optimal source. The slot array operates around a narrow bandwidth centered at 2.9 GHz where it achieves an efficiency that is within 10% of the theoretical bound [Fig. 4(a)]. Figure 4(b) shows that the structure consists of a 2×2 array of cross slots curved at a radius that corresponds to the outer current path. By exciting the structure at the indicated ports [Fig. 4(b), red dots] with the appropriate magnitude and phase, the three primary current paths can be reproduced. Note that the strong currents along the edges of the slots do not contribute to power transfer since they are always paired with currents flowing in the opposite direction.

The position of the device is often not known precisely or subject to displacement due to natural body motion (e.g., heartbeat or breathing). Figure 4(a) shows that efficiency degrades rapidly with displacement, particularly for shifts outside the focal point. For the slot array, this problem can be mitigated by adjusting the phase of each element in the array to change the focal point [Fig. 4(a) inset]. The phase adjustment can be performed electronically so that, with an appropriate feedback mechanism, the system is insensitive to large variations in the device position.

We note that while the efficiencies are inherently low (less than 10^{-4}) due to the small size of the receiver, source optimization is important to obtain operationally useful levels of power. A conservative estimate for the power consumption of a tiny medical device is 10 μW (the pacemaker reported in Ref. [29], for example, consumes 8 μW). For typical applications, the output power of the source is limited to 0.5–2 W in order to ensure that tissue heating falls below thresholds specified for general safety [30]. It is, thus, essential for the system to operate with efficiency greater than 10^{-5} in order for the system to be practical. Such levels of performance are readily obtained by the source presented here at centimeter distances.

Conclusion.—We show that by representing the source as an in-plane current density, an optimal source that bounds the efficiency of power transfer to a weakly coupled device can be derived. Analysis of the source provides insight on the global maximum of an otherwise nonanalytical optimization problem. The method could have application to other electromagnetic source problems, such as the design of optical antennas [31] or focusing with metamaterials [32].

In the present example, we identify an advantageous midfield region for powering an autonomous device. We show that the theoretical bound far exceeds the efficiencies obtained by conventional designs and can be approached closely in practice by a slot-array source. The optimized system delivers useful levels of power to micrometer-scale devices at centimeter depths, which represents a fundamentally new capability. While the study is based on a simple multilayer tissue structure, numerical studies suggest that the conclusions remain valid in more complex tissue geometries (see Ref. [12]).

*adapoon@stanford.edu

[1] K. Vollmers, D. R. Frutiger, B. E. Kratochvil, and B. J. Nelson, Appl. Phys. Lett. **92**, 144103 (2008).
[2] W. H. Ko, S. P. Liang, and C. D. F. Fung, Med. Biol. Eng. Comput. **15**, 634 (1977).
[3] N. N. Donaldson and T. Perkins, Med. Biol. Eng. Comput. **21**, 612 (1983).
[4] U.-M. Jow and M. Ghovanloo, IEEE Trans. Biomed. Circuits Syst. **1**, 193 (2007).
[5] B. Lenaerts and R. Puers, Biosens. Bioelectron. **22**, 1390 (2007).
[6] A. K. RamRakhyani, S. Mirabbasi, and M. Chiao, IEEE Trans. Biomed. Circuits Syst. **5**, 48 (2011).

[7] A. Kurs, A. Karalis, R. Moffatt, J. D. Joannopoulos, P. Fisher, and M. Soljačić, Science **317**, 83 (2007).
[8] A. Karalis, J. D. Joannopoulos, and M. Soljačić, Ann. Phys. (Amsterdam) **323**, 34 (2008).
[9] X. Yu, S. Sandhu, S. Beiker, R. Sassoon, and S. Fan, Appl. Phys. Lett. **99**, 214102 (2011).
[10] Y. Urzhumov and D. R. Smith, Phys. Rev. B **83**, 205114 (2011).
[11] A. A. Rangelov, H. Suchowski, Y. Silberberg, and N. V. Vitanov, Ann. Phys. (Amsterdam) **326**, 626 (2011).
[12] S. Kim, J. S. Ho, L. Y. Chen, and A. S. Y. Poon, Appl. Phys. Lett. **101**, 073701 (2012).
[13] A. S. Y. Poon, S. O'Driscoll, and T. H. Meng, IEEE Trans. Antennas Propag. **58**, 1739 (2010).
[14] S. Gabriel, R. W. Lau, and C. Gabriel, Phys. Med. Biol. **41**, 2271 (1996).
[15] V. Raicu, Phys. Rev. E **60**, 4677 (1999).
[16] S. Kim, J. S. Ho, and A. S. Y. Poon, IEEE Trans. Antennas Propag. **60**, 4838 (2012).
[17] R. F. Harrington, *Time-Harmonic Electromagnetic Fields* (IEEE, New York, 2001).
[18] See Supplemental Material at http://link.aps.org/supplemental/10.1103/PhysRevLett.110.203905 for additional information.
[19] A. Grbic, L. Jiang, and R. Merlin, Science **320**, 511 (2008).
[20] C. Navau, J. Prat-Camps, and A. Sanchez, Phys. Rev. Lett. **109**, 263903 (2012).
[21] I. Rata, A. A. Shvartsburg, M. Horoi, T. Frauenheim, K. W. Michael Siu, and K. A. Jackson, Phys. Rev. Lett. **85**, 546 (2000).
[22] T. Feichtner, O. Selig, M. Kiunke, and B. Hecht, Phys. Rev. Lett. **109**, 127701 (2012).
[23] H. A. Haus, *Waves and Fields in Optoelectronics* (Prentice-Hall, Englewood Cliffs, NJ, 1984).
[24] V. Poor, IEEE Trans. Inf. Theory **29**, 677 (1983).
[25] All necessary codes written in MATLAB can be made available upon request.
[26] For all physical sources, including the coils and slot array, we solve Maxwell's equations using the method-of-moments (IE3D, Mentor Graphics).
[27] The time evolution of the optimal current density is included as a video in the Supplemental Material [18].
[28] E. E. Orlova, J. N. Hovenier, T. O. Klaassen, I. Kašalynas, A. J. L. Adam, J. R. Gao, T. M. Klapwijk, B. S. Williams, S. Kumar, Q. Hu, and J. L. Reno, Phys. Rev. Lett. **96**, 173904 (2006).
[29] L. S. Y. Wong, S. Hossain, A. Ta, J. Edvinsson, D. H. Rivas, and H. Naas, IEEE J. Solid-State Circuits **39**, 2446 (2004).
[30] IEEE standard for safety with respect to human exposure to radio frequency electromagnetic fields, 3 kHz to 300 GHz (1999).
[31] P. Biagioni, J. S. Huang, L. Duò, M. Finazzi, and B. Hecht, Phys. Rev. Lett. **102**, 256801 (2009).
[32] A. Ludwig, C. D. Sarris, and G. V. Eleftheriades, Phys. Rev. Lett. **109**, 223901 (2012).